PHILOSOPHICAL TRANSACTIONS A

rsta.royalsocietypublishing.org

Research

**Cite this article:** McCarthy C, Savage H, Nettles M. 2017 Temperature dependence of ice-on-rock friction at realistic glacier conditions. *Phil. Trans. R. Soc. A* **375**: 20150348. http://dx.doi.org/10.1098/rsta.2015.0348

Accepted: 17 August 2016

One contribution of 11 to a theme issue 'Microdynamics of ice'.

**Subject Areas:**
glaciology

**Keywords:**
frictional healing, glaciers, basal sliding, ice friction

**Author for correspondence:**
C. McCarthy
e-mail: mccarthy@ldeo.columbia.edu

# Temperature dependence of ice-on-rock friction at realistic glacier conditions

C. McCarthy, H. Savage and M. Nettles

Lamont-Doherty Earth Observatory, Columbia University, New York, NY, USA

CM, 0000-0002-5276-5246

Using a new biaxial friction apparatus, we conducted experiments of ice-on-rock friction in order to better understand basal sliding of glaciers and ice streams. A series of velocity-stepping and slide–hold–slide tests were conducted to measure friction and healing at temperatures between −20°C and melting. Experimental conditions in this study are comparable to subglacial temperatures, sliding rates and effective pressures of Antarctic ice streams and other glaciers, with load-point velocities ranging from 0.5 to 100 $\mu m\,s^{-1}$ and normal stress $\sigma_n = 100$ kPa. In this range of conditions, temperature dependences of both steady-state friction and frictional healing are considerable. The friction increases linearly with decreasing temperature (temperature weakening) from $\mu = 0.52$ at −20°C to $\mu = 0.02$ at melting. Frictional healing increases and velocity dependence shifts from velocity-strengthening to velocity-weakening behaviour with decreasing temperature. Our results indicate that the strength and stability of glaciers and ice streams may change considerably over the range of temperatures typically found at the ice–bed interface.

This article is part of the themed issue 'Microdynamics of ice'.

## 1. Introduction

The motion of many glaciers and ice streams is controlled by frictional properties at the bed, which determine whether and how easily basal sliding will occur. Reliable sea-level-rise projections require an improved understanding of ice flow, in particular the slip at the ice–bed interface, which is currently one of the least understood aspects of glacier dynamics. Processes taking place at the ice–bed interface are poorly constrained by

THE ROYAL SOCIETY PUBLISHING

observation. *In situ* field measurements at the bed, from boreholes and tunnels, are very limited in spatial and temporal extent, while bed conditions are expected to vary considerably in time and space (e.g. [1]). Efforts to obtain sliding rules from field measurements have failed to identify a consistent relationship describing observed flow rates over time [2]. Variations in sliding style, including smooth sliding, stick–slip behaviour, slowdowns and switches of flow state, are attributed to basal processes (e.g. [3–6]) but are not well understood. A clearer understanding of the controls on sliding rate, including time, temperature and other basal characteristics, is essential to next-level modelling and forecasting.

Temperature at the base of the glacier is controlled by heat conduction in response to geothermal heat flux, strain heating within the ice and climate history (e.g. [7]), and has a clear role in determining the mode and rate of glacier deformation. Herein, we will use the term glaciers to represent all bodies of ice sliding over a substrate. Warm-based glaciers, those that are above or at their melting point at the ice–bed interface, are thought to deform by a combination of viscous flow and basal sliding. The sliding may be tied to the geometry and flow conditions of a basal hydrological system. Cold-based glaciers, below freezing at the interface, are thought to be frozen to the bed, deforming through viscous flow in the bulk of the glacier only, rather than through basal sliding. Glacier sliding is in part controlled by friction of the glacier at the bed, most probably at the ice–till interface, within the till itself, or at the ice–bedrock interface when till is absent or variable (e.g. [7]). The frictional interface on which glaciers slide is in many ways similar to a tectonic fault, and ice sliding over the glacier bed should follow the same rate- and state-dependent behaviour as tectonic faults, albeit with the temperature dependences appropriate to the rate-limiting micromechanisms at glacier conditions.

Previous experimental studies have elucidated important physics related to the velocity and temperature dependences of laboratory grown and natural ice-on-ice friction [8–14], ice-on-rock friction [15–17] and till friction [18] over a broad range of conditions. However, only a few studies [12,14,16] utilize the formalism of rate- and state-dependent frictional behaviour that is common in rock mechanics, and which may provide a useful framework for assessing stability and sliding behaviour of glaciers.

In this study, we perform laboratory experiments to explore the friction parameters of ice–rock interfaces, presenting our results in the framework of rate- and state-dependent frictional sliding. We choose a pure-ice–rock interface, which is an end member condition for the many complexities that may control glacier sliding in the natural world. Building on previous work that was conducted at a more limited temperature range [16], we focus on the first-order controls of temperature on strength and stability of ice–rock friction over the range of temperatures found at the base of glaciers and ice sheets. Information about these parameters will provide a needed comparison for field observations, and will aid in the modelling and forecasting of glacier flow rates.

## 2. Background

The complexities of frictional sliding in laboratory experiments are well characterized by rate- and state-dependent constitutive friction laws [19–22]. These laws describe the dependence of friction on sliding velocity and fault state (the time dependence of friction). This framework has been successfully applied to explain multiple aspects of fault slip including earthquake rupture, repeating earthquakes, slow slip events and afterslip [23–26]. Glaciers exhibit similar slip behaviours to faults, but to date there has been more limited application to glacial sliding [16,18]. The rate–state constitutive equations specify that friction is a function of sliding velocity and state, such that

$$\mu = \frac{\tau}{\sigma_{\mathrm{n}}} = \mu_0 + a \ln\left(\frac{V}{V_0}\right) + b \ln\left(\frac{V_0 \theta}{D_{\mathrm{C}}}\right), \tag{2.1}$$

$$\frac{\mathrm{d}\theta}{\mathrm{d}t} = 1 - \frac{V\theta}{D_{\mathrm{C}}} \tag{2.2}$$

and $$\frac{\mathrm{d}\theta}{\mathrm{d}t} = -\frac{V\theta}{D_C}\ln\left(\frac{V\theta}{D_C}\right), \tag{2.3}$$

where $\tau$ and $\sigma_n$ are shear and normal stresses, respectively, $V$ is sliding velocity, $\theta$ is a state variable that describes contact lifetime, $D_C$ is the critical slip distance that is needed for the system to evolve from one steady-state friction to another [27], and parameters $\mu$, $a$ and $b$ are experimentally determined coefficients. Equations (2.2) and (2.3) are two different forms of the state evolution. Equation (2.2) states that contact evolution can take place even under stationary contact [19], whereas in equation (2.3) the state variable can only evolve while slipping [21].

The microstructural reasons for time-dependent slip and healing are not entirely understood. In rocks sliding at relatively low homologous temperature ($T/T_m < 0.6$) the mechanisms are believed to be plasticity and diffusion at asperities and subcritical fracture, all of which are thermally activated processes [28,29]. In terrestrial glaciers (and in our study), homologous temperatures are $T/T_m > 0.9$. The dominant mechanism(s), and therefore the time and temperature dependence, are expected to be considerably different.

## 3. Experimental method

Polycrystalline ice samples were prepared using an adaptation of the 'standard ice' method [30]. In this method, seed ice was ground and sieved between 108 and 250 µm mesh, and packed, in this case into a rectangular aluminium die. After an equilibrium period held within a zero degree ice bath, a vacuum was pulled on the packed seeds and deionized water was slowly flooded from the bottom to fill the pore spaces. The two-phase mixture was then placed on a cold plate in a freezer (−5°C) with insulation around the sides so that the sample slowly froze from the bottom up, resulting in nominally pore-free (less than 1%) polycrystalline ice, which, after approximately 48 h at −5°C, experienced grain growth to a uniform grain size of approximately 1.5 mm (figure 1 inset). The die is intentionally oversized and the sample was cut down to 50 × 50 × 100 mm with a microtome housed in a cold room (−17°C). The sliding surfaces were roughened with a no. 100 grit sandpaper to a roughness average (R$a$) of $7 \pm 1$ µm as determined by a profilometer (Mitutoyo SF-210). A single grain size was employed in this study because previous studies of ice-on-ice friction showed no grain size dependence in the range of 2.5–6.0 mm [11].

The sample assembly for this study consisted of a double-direct-shear configuration with the ice sample as the central sliding block and two stationary rock samples on the sides (figure 1). The rock type used was Barre granite with a grain size of 1–5 mm. The rock surface was polished with a surface grinder to R$a = 2.8 \pm 2$ µm. The rock pieces sit atop two steel bases that were coated with dry molybdenum powder for frictionless sliding in the horizontal direction. The configuration allows for a maximum of 50 mm slip.

Friction experiments were conducted using a purpose-built ambient pressure, servo-hydraulic, biaxial friction apparatus described more fully in McCarthy *et al*. [31]. The horizontal piston applied the normal stress, and the vertical piston pushed the central ice piece down through the stationary rock pieces at constant load-point velocity. Load cells in the vertical and horizontal pistons (positioned outside the cryostat) and the cross-sectional areas ($50 \times 50\,\mathrm{mm}^2$ and $2 \times (50 \times 50\,\mathrm{mm}^2)$) provided the normal stress and shear stress values, respectively, the ratio of which is friction, $\mu$. Following a run-in at either 5 or 10 µm s$^{-1}$ to a displacement of approximately 4 mm, a combination of velocity steps and slide–hold–slides were conducted (figure 2). Sliding velocity ranged from 0.05 to 100 µm s$^{-1}$. An inverse modelling technique with an iterative least-squares method was used to fit velocity step data to equations (2.1) and (2.3). Employing a single state variable, we calculated the rate dependence of friction with the dimensionless parameter $a$–$b$ (e.g. [32]). This parameter represents the steady-state change in friction with a change in velocity. By rearranging equation (2.1), we obtain

$$a - b = \frac{\Delta\mu_{ss}}{\ln(V/V_0)}, \tag{3.1}$$

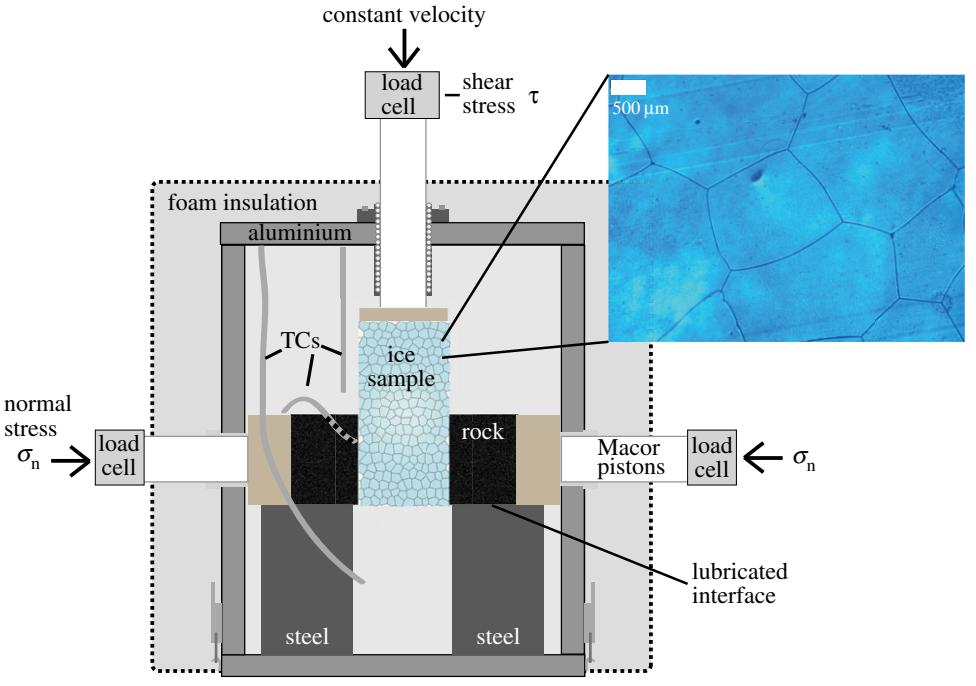


**Figure 1.** Configuration of sample assembly used for ice-on-rock double-direct-shear friction experiments. Thermocouples (TCs) monitoring temperature were mounted within each side, in air above and below the sample, and embedded within the rock at the sliding interface. Temperatures used herein refer to the rock-embedded values. Inset: representative initial microstructure of standard ice sample, with approximately 1.5 mm grain size and less than 1% porosity. (Online version in colour.)

where $\Delta\mu_{ss}$ is the change in steady-state friction upon a change in velocity from $V_0$ to $V$ (e.g. [22]). A material with a positive value of $a$–$b$ is termed velocity strengthening, which indicates a system that will slide stably. A material with a negative value of $a$–$b$ is termed velocity weakening, which indicates that dynamic slip is possible [33].

All runs in this study were conducted at a normal stress $\sigma_n$ of $100 \pm 10$ kPa. We do not explore the effect of normal stress on friction in this study. However, the values measured here at 100 kPa are consistent with that of Zoet *et al*. [16], conducted at 1 MPa. Furthermore, studies of ice-on-ice friction [11,34] have shown no discernible difference in steady-state friction with $\sigma_n$ in the range 20–1000 kPa. We therefore do not expect normal stress to affect the frictional values of the system explored here.

Following the methods of Dieterich [35], Beeler *et al*. [36] and Marone [22], slide–hold–slide tests, which measure frictional healing, were conducted by driving the central sample down at constant load-point velocity and then holding the driving piston stationary for prescribed durations, $t_h$, before resuming downward motion at the initial velocity. The sliding portions of the slide–hold–slide experiments were conducted at either 5 or 10 µm s$^{-1}$ for 100 s and were punctuated by holds of 1, 3, 10, 30, 100, 300 and 1000 s. At the onset of the hold, friction decays nonlinearly from a steady-state value due to relaxation of the sample, the testing apparatus and the assembly (e.g. [19]; figure 2 lower inset). When motion is resumed, friction increases to a maximum value before returning to steady state. We measured frictional healing, $\Delta\mu$, as the difference between the friction peak and the pre-hold steady-state friction and frictional creep relaxation, $\Delta\mu_c$, as the difference between the last value at the end of a hold and the steady-state friction before the hold.

All experiments were run at constant temperature. Temperature was controlled with an insulated aluminium cryostat cooled through a methanol–water mixture passing through heat

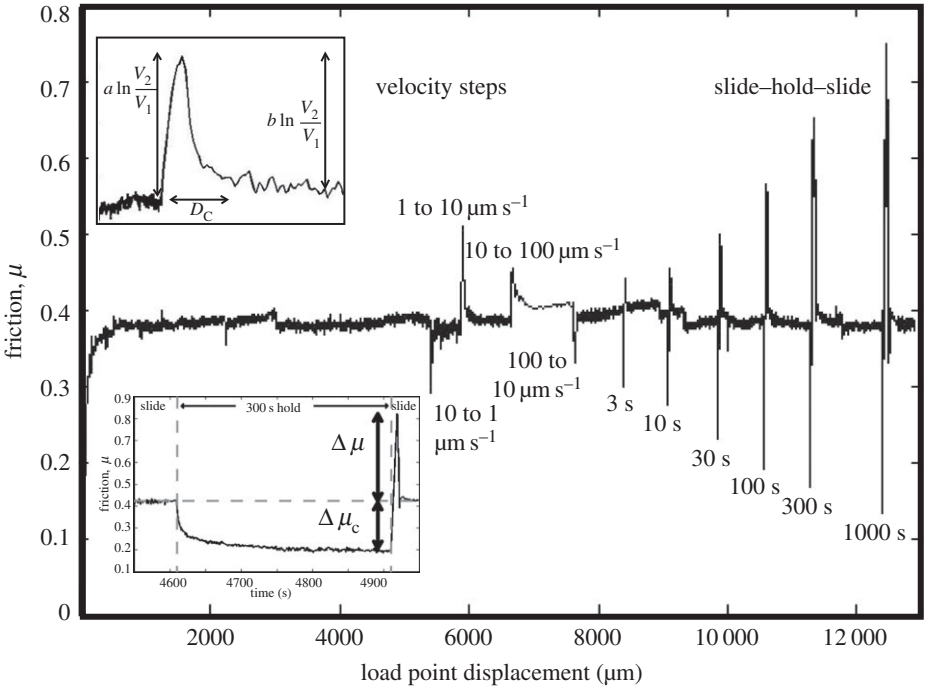


**Figure 2.** Velocity steps and slide–hold–slide tests for polycrystalline standard ice sliding against two granite blocks at $\sigma_n = 100$ kPa and $T = -13$°C. In this run, velocity steps were conducted after a run-in of approximately 5 mm displacement. Holds are labelled below by duration in seconds. Top inset: a single velocity step, which is used to determine rate–state friction parameters (equation (2.1)). Bottom inset: a single segment of a slide–hold–slide test versus time (from the same data as in the main figure) showing the relaxation of friction at the onset of the hold and the friction peak once sliding is reinitiated.

exchangers attached to the outside [31]. Type T thermocouples (with a manufacturer's reported accuracy of ±1.8°C) monitored temperature at multiple locations within the cryostat, including one thermocouple embedded in the rock at the rock–ice interface. Some variation (2–3°C) was measured from top to bottom of the cryostat, so temperatures cited here refer to the temperature of the rock-embedded thermocouple because it represents the temperature at the interface that controls sliding properties. Samples and sliding rocks were allowed to equilibrate at testing temperatures for several hours prior to testing.

Characterization of experimental samples before and after friction tests was performed using a Leica light microscope housed within a cold room (−17°C). Prior to imaging, a mirror finish was obtained on the imaged surface using a microtome. Images were taken in refracted light. Sublimation after microtoming accentuates grain boundaries. From the average of nine positions within each imaged sample, we used the linear intercept method to determine grain size and Fiji image analysis software to determine porosity [37,38].

# 4. Results

## (a) Steady-state friction

Figure 3 and table 1 provide the steady-state friction results for polycrystalline ice sliding on rock as a function of both velocity and temperature. These values are slightly lower than for previously reported ice–rock friction experiments [15] and comparable to those of Zoet *et al.* [16]. At these conditions, there is clear temperature dependence for the steady-state friction at all velocities

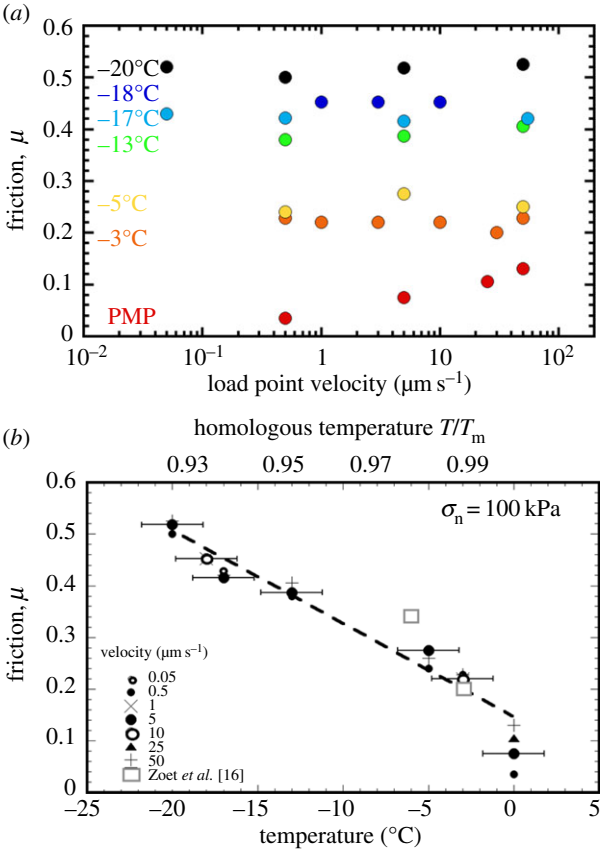


**Figure 3.** Steady-state friction at various velocities and temperatures. (*a*) Clear temperature dependence is observed. PMP is the pressure melting point. Melt was confirmed by microstructure. (*b*) Friction versus temperature/homologous temperature. (Error is that associated with type T TC.) For comparison, plot shows results from Zoet *et al.* [16], who also measured ice sliding on granite at 10 μm $s^{-1}$, but at $\sigma_n = 1.25$ MPa. A linear fit through all of the data shows that friction is dependent on inverse temperature as $-0.0182°C^{-1}$ (dashed line).

(figure 3*a*). The range in friction coefficients (from 0.52 to 0.02) is significant over a homologous temperature range of 0.93 to approximately 0.99. In this range, friction is linearly dependent on temperature as $-0.0182°C^{-1}$ (figure 3*b*).

## (b) Frictional healing

Results of slide–hold–slide tests are shown in figure 4. Frictional healing $\Delta\mu$ in rocks has been shown to increase linearly with the logarithm of the hold time as $\beta = \Delta\mu/\log(\text{time})$ (e.g. [22,35]). As is the case with rock friction [39], we find healing is proportional to frictional strength, with the coldest samples exhibiting the highest friction and greatest healing (figure 4*a*). However, although the coldest temperatures of ice have steady-state friction values similar to those of many rock types (approx. 0.5), the measured frictional healing in ice in this temperature range spans a much greater range and, at its highest, is orders of magnitude greater than that measured in rock. Similar large healing values have been observed in ice-on-ice friction experiments in the range of glacier temperatures [12] and in debris-laden ice [16]. The slope of a line connecting $\Delta\mu$ values as a function of hold times is considered the healing rate, $\beta$. We measured $\beta$ between holds of 3 and 1000 s. The data shown here on a log-linear plot are slightly concave up, particularly at colder temperatures, suggesting a better fit to log-log, which will be described below. $\beta$-values decrease

**Table 1.** List of experiments, conditions and measured steady-state friction values.

| experiment no. | temp (°C)[a] | velocity ($\mu$m s$^{-1}$) | ss-friction $\mu_{ss}$ |
|---|---|---|---|
| C0017 | −17 | 0.05 | 0.43 |
| | | 0.5 | 0.422 |
| | | 5 | 0.415 |
| | | 50 | 0.42 |
| C0018 | −13 | 0.5 | 0.38 |
| | | 5 | 0.389 |
| | | 50 | 0.405 |
| C0019 | −20 | 0.05 | 0.52 |
| | | 0.5 | 0.50 |
| | | 5 | 0.518 |
| | | 50 | 0.525 |
| C0020 | −5 | 0.5 | 0.24 |
| | | 5 | 0.275 |
| | | 50 | 0.250 |
| C0021 | PMP | 0.5 | 0.035 |
| | | 5 | 0.075 |
| | | 25 | 0.105 |
| | | 50 | 0.130 |
| C0026 | −18 | 1 | 0.452 |
| | | 3 | 0.452 |
| | | 10 | 0.452 |
| C0027 | −3 | 0.5 | 0.228 |
| | | 1 | 0.22 |
| | | 3 | 0.22 |
| | | 10 | 0.22 |
| | | 30 | 0.22 |
| | | 50 | 0.228 |

[a]Temperatures are based on the reading from the type T thermocouple embedded in the rock to the rock–ice interface. Manufacturer's error for this sensor is ±1.8°C.

with temperature as 0.0089°C$^{-1}$ and range from $\beta = 0.0085\ \Delta\mu$ per decade (at the pressure melting point (PMP)) to $\beta = 0.20\ \Delta\mu$ per decade (at −20°C) (figure 4*b*). Creep relaxation $\Delta\mu_c$ as a function of hold time and temperature is shown in figure 5*a*. As with healing, those samples with higher friction (i.e. those at lower temperature) demonstrate higher rates of relaxation.

In order to explore the relationship between healing and relaxation, we plot the ratio of $\Delta\mu$ to $\Delta\mu_c$ (figure 5*b*). Upon reloading the sample after the longest holds at the coldest temperatures, one or two stick–slips occurred before the system returned to steady state. In figure 5*b*, we show which holds demonstrated stick–slip behaviour (symbols with thick black outlines). In general, the onset of stick–slip corresponds to the conditions (colder, longer holds) in which healing $\Delta\mu$ is greater than relaxation $\Delta\mu_c$, that is, when the ratio plotted in figure 5*b* is larger than 1. Previous studies of ice-on-ice friction observed stick–slip at all times when velocities were $\geq 50\,\mu\mathrm{m\,s}^{-1}$

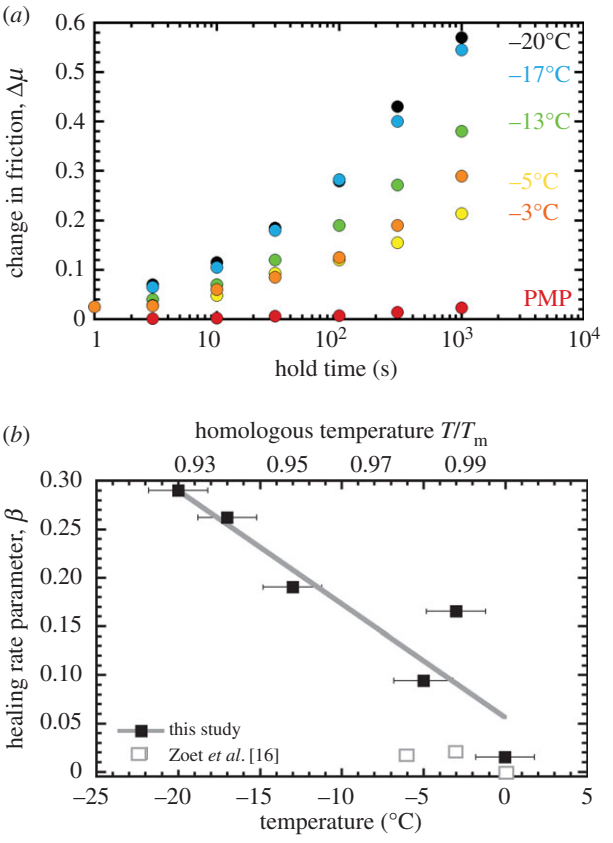


**Figure 4.** Results of slide–hold–slide tests: (*a*) change in friction following a hold versus time of the hold. As with the steady-state friction, clear temperature dependence is observed with the lowest temperatures displaying the highest healing. (*b*) Healing rate, $\beta$, versus temperature/homologous temperature. A linear fit through the data from this study shows a dependence of healing on inverse temperature as 0.0089°C$^{-1}$. Results from Zoet *et al.* [16] are shown for comparison.

[10,11]. At the fastest velocities (30 and 100 µm s$^{-1}$), the experiment at −18°C displayed regular stick–slip instabilities.

## (c) Velocity dependence of ice friction

We determine the rate dependence of ice friction (*a*–*b*) through an inverse fit of the experimental velocity steps using equations (2.1) and (2.3) and an iterative least-squares fitting procedure. We find a significant temperature control on the rate dependence (figure 6 and table 2). Colder temperatures are more likely to exhibit velocity-weakening behaviour at most or all velocities, with the transition from velocity strengthening to velocity weakening occurring around −15°C. However, we expect that the transition temperature will be highly dependent on sliding velocity and additional experiments are needed to explore more fully the velocity dependence of *a*–*b* at isothermal conditions. Previous experiments have demonstrated that velocities in the range 10–300 µm s$^{-1}$ can exhibit velocity-weakening behaviour at temperatures as high as −3 to −6°C [16].

## (d) Microstructure

An example of the initial, as-fabricated microstructure of the ice samples we use is shown in the inset of figure 1. Classic foam texture is observed with uniform grain size of approximately

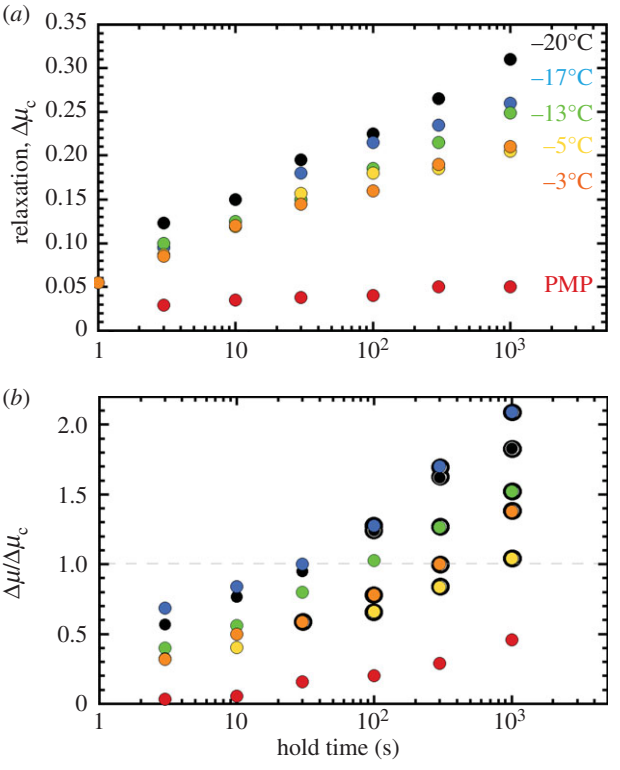


**Figure 5.** (*a*) Relaxation $\Delta\mu_c$ versus hold time, as a function of temperature. (*b*) Ratio of healing to relaxation $\Delta\mu/\Delta\mu_c$ versus temperature. Dark outlines around symbols denote those holds demonstrating a stick–slip upon reload. In general, the onset of stick–slip corresponds to the conditions (colder, longer holds) in which healing exceeds relaxation (i.e. more than 1; denoted by the dashed line).

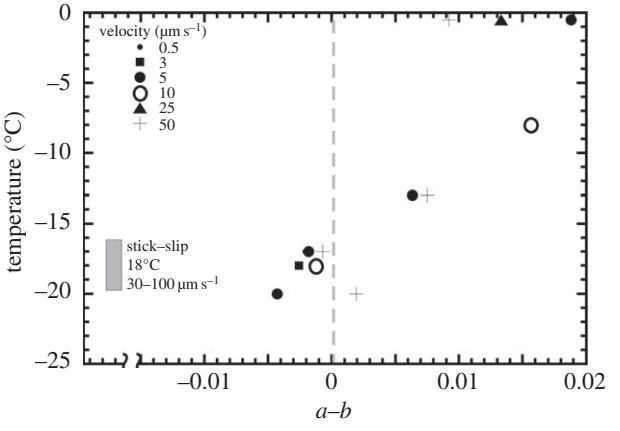


**Figure 6.** Rate dependence of friction, *a*–*b*, versus temperature at various velocities. At 18°C (±1.8°C), we observed stick–slip behaviour at 30 and 100 μm s$^{-1}$, which is indicated by the grey shaded box. The general trend is from negative *a*–*b* (velocity weakening) at the lowest temperatures to positive *a*–*b* (velocity strengthening) at higher temperatures, with the transition at approximately −15°C.

1.5 mm. Grains are generally equiangular and polygonal, with porosity less than 1%. Images of samples after testing indicate that for the sample tested at approximately the PMP, although the interior grains are nearly identical to the as-fabricated grains (figure 7*a*), the sliding

**Table 2.** Velocity dependence of frictional strength (shown in figure 6) as determined from fitting to rate–state equations.

| experiment no. | $T$ (°C) | velocity step | $a-b$ |
|---|---|---|---|
| C0010 | −8 | 1–10 | 0.0157 |
| C0017 | −17 | 0.05–0.5 | −0.00210 |
| | | 0.5–5 | −0.00182 |
| | | 5–50 | −0.00074 |
| C0018 | −13 | 0.5–5 | 0.00634 |
| | | 5–50 | 0.0075 |
| C0019 | −20 | 0.5–5 | −0.0043 |
| | | 5–50 | 0.0019 |
| C0021 | PMP | 0.5–5 | 0.0188 |
| | | 5–25 | 0.0133 |
| | | 5–50 | 0.0092 |
| C0026 | −18 | 1–3 | −0.0026 |
| | | 3–10 | −0.0013 |

interface consisted of elongated grains (perpendicular to the sliding direction), consistent with recrystallized melt (figure 7*b*). Water found at the base of the cryostat confirmed melting. Images of those samples tested at temperatures lower than the PMP demonstrate uniform grain size extending from the interior to the sliding edge (figure 7*c*), indicating no melting occurred. Circular roughness patterns from the initial preparation were still visible macroscopically on the entire length of the sliding faces for those samples tested below melting (figure 8), though the portion of the surface that slid against rock had some larger grains visible and patches where the circular roughening patterns were less evident (figure 8*b*). Roughness measurements indicate that the part of the sliding surface that did not slide during the experiment (the top approximately 20 mm) had a post-test $Ra = 3.82 \pm 1.04$ µm, whereas the area that slid had $Ra = 1.20 \pm 0.3$ µm (compared with initial $Ra = 7 \pm 1$ µm). Some smoothing of the entire surface is probably due to sublimation, but the difference between slid and not-slid surfaces is distinct. No surface fractures or visible wear or gouge were observed in any of the tested samples.

## 5. Discussion

The frictional behaviour of ice has long been known to be greatly dependent on temperature and velocity [15,40], with a complicated 'map' of frictional behaviour over temperature–velocity space. At very high velocities (more than $10^{-3}$ m s$^{-1}$) and temperatures (more than −10°C), frictional heating is great enough to melt the ice surface and provide a lubricating film, providing very low friction [8,41,42]. At very low temperatures (less than −100°C), frictional sliding has been attributed to elastically deforming asperities that undergo shear failure [10]. Intermediate speeds (approx. $10^{-5}$ to $10^{-4}$ m s$^{-1}$) have shown the highest frictional values (e.g. [12,15]. Temperatures at the base of all terrestrial glaciers and ice sheets are believed to be within the range of −20°C and melting (e.g. [7]). And although rates of ice motion vary considerably from a few centimetres per year near the ice divides to a few kilometres per year on fast-moving glaciers and floating ice shelves [43], it is in this intermediate range (100–300 m year$^{-1}$ or approximately $10^{-5}$ m s$^{-1}$) that many ice streams flow. The fast-moving ice streams are currently demonstrating the most rapid change over the widest area, and represent the greatest impact on total ice sheet mass balance [44]. Therefore, for this study, we have focused on relatively high temperatures and velocities, those appropriate to terrestrial ice streams, in order to provide frictional values for ice sliding

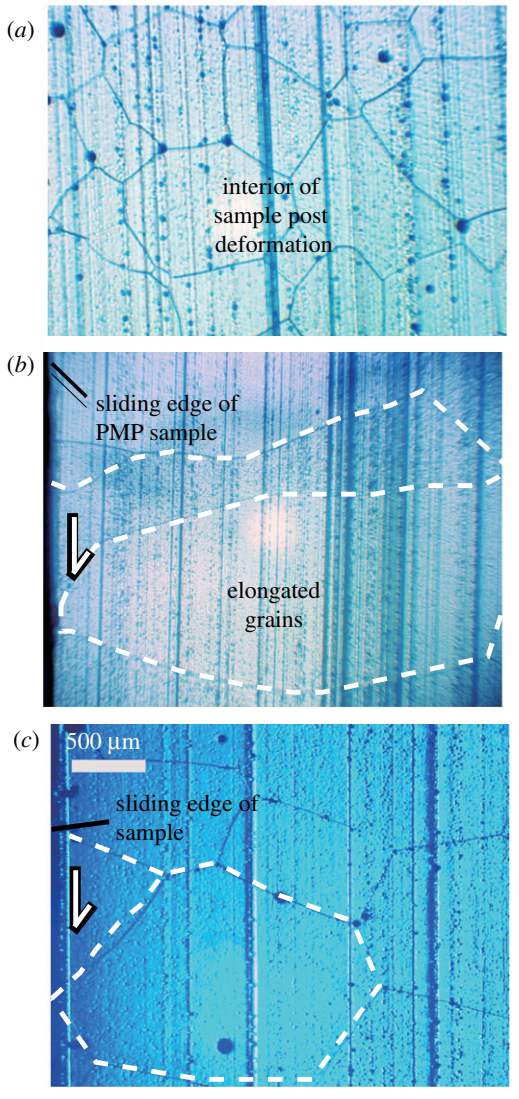


**Figure 7.** Light microscope images of two samples post testing. (*a*) Grain interior of the PMP sample is nearly identical to the as-fabricated sample (figure 1 inset); (*b*) cross-section image of the sliding edge of PMP sample shows large, elongated grains consistent with melt and recrystallization (rock would be stationary and to the left of the image). (*c*) Cross-section image of the sliding edge of a sample (tested at −3°C) that did not melt. Polygonal foam texture extends to the edge indicating no melting/recrystallization. No visible cracking was present. Long straight lines in all images are due to microtome cuts during imaging preparation. Dashed white lines outline individual grains. (Online version in colour.)

on rock as a function of temperature that can be used in predictive models of flow, stability and mass balance.

Our results, like those of previous studies (e.g. [16]), show that ice–rock friction follows the same rate–state-dependent laws that govern fault mechanics. Although velocity dependence of friction is significantly smaller than temperature dependence, it determines the sliding style. By analysis of velocity steps, we discern temperature dependence for the transition from velocity-strengthening to velocity-weakening behaviour (figure 6). Temperature dependence of friction has been observed in certain rock/gouge types (e.g. [45–48]). The ability of the different rock types to heal is a function of the overall strength [29,39]. Our experiments, through variation in temperature instead of rock type, show a similar result. The temperature dependence of

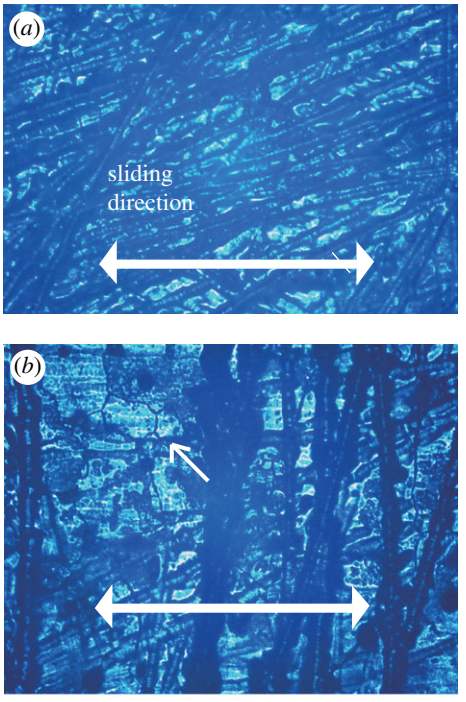


**Figure 8.** Light micrograph images of a sample after testing, looking in the direction normal to sliding, at conditions below the melting temperature. Random criss-crossing striations from sample roughening are clearly evident. Panel (*a*) is an uppermost portion of that face that did not slide during the test (we did not run the full 50 mm that the sample size allows). Panel (*b*) is a portion that slid. In (*b*), striations are still visible but many have been overprinted by grain growth, possibly capturing the direction of sliding (small arrow). (Online version in colour.)

steady-state friction and healing yield similar values, implying that the increase in healing with decreasing temperature is a function of the overall strength of the interface. However, the temperature dependences of friction and healing described here are at least 10 times greater than that observed for rocks. The homologous temperatures explored here (and experienced by terrestrial glaciers) are much higher ($T/T_m > 0.93$) than those explored in rock friction studies and we expect the dependences and mechanisms to be different.

Figure 9 provides an indication of the mechanisms controlling friction and healing. We plot frictional healing $\beta$ from our study and those of several other ice and rock studies as a function of homologous temperature. By plotting in this way, a general trend and grouping of high and low healing with homologous temperature becomes apparent. The different regions (separated with the dashed lines) are probably due to different healing/friction mechanisms, as follows.

At high homologous temperature (essentially 1) are experiments that were conducted at the pressure melting temperature. These show very low healing rates (figure 9). In these samples, a layer of melt at the interface must inhibit contact growth and cohesion needed for healing. In these studies, the melt was produced because of the temperature and the normal stress. The PMP comes from the Clausius–Clapeyron equation, and for ice is $\Delta T_{PMP}/\Delta P = 0.078^\circ\,\mathrm{MPa}^{-1}$. However, depression of the melting temperature calculated using the pressure with the entire sliding surface area $A$ is very small (less than 1°C). We observed melting at temperatures lower than this (more than −3°C), suggesting pressure concentrated at the real area of contact (that of asperities) $A_r$ is important. (A more detailed exploration of melting due to frictional heating and contact area is planned, but is beyond the scope of this paper.) Some studies at lower temperatures have achieved comparable low friction with high velocities that result in frictional

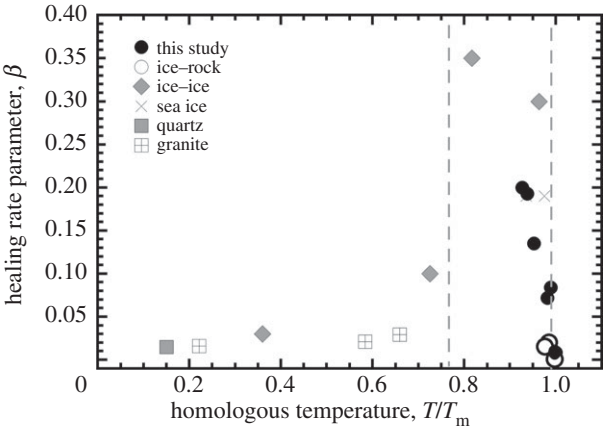


**Figure 9.** Healing rate versus homologous temperature from this study and other studies on ice and rock. Ice–rock data at PMP from Zoet *et al*. [16]; ice–ice data from Schulson & Fortt [12]; sea ice from Sukhorukov & Loset [49] Quartz from Katayama *et al*. [50]; and granite from Nakatani [51] and Mitchell *et al*. [46]. All other data are from this study.

heating sufficient to produce a drop in friction [15,42]. The presence of a fluid film over what is probably the entire sliding interface lubricates it, greatly reducing the frictional resistance.

In the high homologous temperature range (but below melting; figure 9) is a region displaying the highest healing levels. These data are from our study of ice–rock and other studies of ice–ice [12,52]. In this regime, healing probably occurs as the contact area of asperities increases due to high-temperature creep (e.g. dislocation creep). The increase in area with hold time thereby creates an increase in shear resistance to sliding. The reduced roughness we observe on the sliding surface for these samples is an indication that, during the experiment, the grooves made from roughening with sandpaper were relaxed. The curvature in the lines of the log-linear plot of figure 4*a* indicates that the mechanism for healing is probably not the low-temperature exponential mechanism(s) typical of rock friction, but rather a power-law form consistent with high-temperature deformation of ice. This finding is consistent with the asperity creep-based model put forth in [11] and [12], and described in more detail by Schulson [52] in which deformation within a narrow surface zone predicts a power-law dependence of $\Delta\mu$ on hold time. Their model relates the ratio of the real area of contact to apparent area, $A_r/A$, to hardness, which thus provides the same inverse temperature dependence observed here. Although the healing at this high homologous temperature is related to high-temperature power-law creep (e.g. dislocation creep), the sliding itself is still in a frictional regime in which $\tau = \mu\sigma_n$, as evidenced by similar friction values between our study and those of [16] (which were at $\sigma_n = 1$ MPa). Theoretically, at high enough normal stress, this would cease to be the case and the system would transition to a fully viscous process of sliding, but we do not observe that transition here. Importantly, we do not see evidence of melting and refreezing, nor of microcracking in this high homologous temperature regime below the melting temperature, which are mechanisms suggested by theory and previous studies. Rather, our indication from samples tested from −20°C to −3°C is that they slide frictionally, without the aid of a melt layer, and display a measurable friction coefficient that varies linearly with temperature.

As Schulson & Fortt [12] point out, the inverse temperature dependence of healing breaks down at intermediate temperatures (arbitrarily drawn in figure 9 at $T/T_m \approx 0.76$) and the reverse is observed. At homologous temperatures lower than approximately 0.7 healing rates in ice are low and similar to those of rock. At such low homologous temperatures, healing has been attributed to low-temperature exponential creep of asperities (e.g. pressure solution) (e.g. [29]). In studies of ice sliding on ice at low homologous temperature, friction was found to be independent

of temperature, roughness and sliding rate, and under those conditions a purely elastic–brittle mechanism for friction has been posited, related to fracture [9,10,12].

In addition to shedding light on behaviour at the base of glaciers, these results have implications for the base of the seismogenic zone in faults and below, where the transition from velocity weakening to velocity strengthening is not well known. As $T/T_m > 0.9$ is difficult to obtain in studies on rock, ice can act as an analogue to study frictional strength and whether ruptures can penetrate to those depths.

## 6. Implications for glaciers

The experiments run here were conducted at conditions of normal stress, temperature range and velocity comparable to glaciers and ice streams. Frictional interfaces at actual glaciers are more complex, with substrates that vary from entrained debris to distinct frozen or wet till layers. These variations in sliding interface will be systematically explored in future studies. However, this study provides temperature and velocity dependences in a simplified system, which provides initial constraints on frictional behaviour at the ice–rock interface.

The clear temperature dependence of steady-state ice friction has implications for the conditions under which basal sliding can occur. Normal stress at the glacier bed is controlled by the weight of the overlying glacier minus the pore pressure at the base, so that the effective normal stress is often of the order 10–100 kPa [7]. The driving force for sliding is the gravitational potential of the upstream ice and is typically around 50–150 kPa, but with considerable variability and a range from approximately 10 to approximately 400 kPa [7]. The results in figure 3 and the relationship $\tau = \mu(T)\sigma_n$ can be used to determine whether sliding can occur assuming ice sliding on bedrock. For instance, with an effective normal stress of 100 kPa and a driving stress of 50 kPa, a glacier could slide at temperatures as low as approximately −18°C. For a driving stress of 20 kPa, the temperature would need to be above approximately −3°C in order for frictional sliding to occur. The temperature dependence of ice–rock friction has important implications for deformation of warm- and cold-based glaciers, though to fully understand glacial deformation we clearly need a more thorough understanding of ice rheology in addition to frictional characteristics over the appropriate temperature range.

Earthquakes at the glacier bed have been observed in ice-stream [53,54], outlet-glacier [5,55] and mountain-glacier [56] settings. Most authors interpret these events to be the result of stick–slip behaviour at 'sticky spots', which are believed to be analogous to asperities on tectonic faults, though some basal events probably result from crack opening or closing [57]. We expect our results to help inform interpretation of these earthquakes and their role in glacier deformation, particularly as many such events appear to occur where bedrock rises or changes in topography may result in thinner or no till at the bed. Some of the best-known basal-sliding events, those reported at Whillans Ice Stream in Antarctica by Bindschadler *et al*. [58] and later workers (e.g. [59–62]), appear to show healing behaviour qualitatively similar to that we observe in our laboratory results. Following a large 'hold', or stuck phase, slip events at Whillans are larger than after short holds [60]. The slip behaviour there appears to have evolved over the last several years [61], for reasons that are not yet completely clear. Accounting for viscoelastic [63] and other effects, such as till compaction [6,64], will also be important in this setting, but our results provide constraints that will allow progress beyond previous, necessarily simplified, models [60] of the intriguing behaviour of the Whillans Ice Stream and other glacier stick–slip settings. Our results will also aid in inference of bed properties from macroscopic observations of sliding style. In particular, the very high healing rates we observe even in the absence of till or debris should inform interpretation of a wide range of glacier stick–slip events.

## 7. Conclusion

Our laboratory experiments demonstrate that changes in temperature over the range from −20°C to the PMP exert a first-order effect on ice-on-rock friction. Steady-state friction increases with

decreasing temperature at a rate of $0.018°C^{-1}$, while frictional healing increases with decreasing temperature at a rate of $0.0089°C^{-1}$. The healing rate, $\beta$, is greater than that found for rocks, including for rocks at large values of homologous temperature. Microstructural evidence of melt is present at the PMP, but is absent at the other temperatures we study. Healing below the PMP thus appears to be due to some process other than melting and refreezing during shear. Velocity-stepping experiments show that ice transitions from velocity-strengthening to velocity-weakening behaviour at approximately −15°C, although the transition is also dependent on sliding speed. Our results indicate that ice friction changes significantly in both strength and stability over the temperature range (−20°C to PMP) observed at the base of glaciers and ice streams on Earth and should be taken into account in interpretation of modes and rates of glacier sliding. Experiments of the type we perform here may also be used to improve understanding of rock-based fault systems near the brittle–ductile transition.

Competing interests. The authors declare that there are no competing interests.

Authors' contributions. C.M., H.S. and M.N. contributed to the original research idea. C.M. collected the data. C.M. and H.S. designed the experiment and analysed the data. C.M. and H.S. drafted the manuscript with input from M.N. and all co-authors gave approval for the manuscript to be published.

Funding. This research was supported by NSF under award no. ANT 1245871. Lamont–Doherty contribution number 8075.

Acknowledgements. The authors thank L. Zoet and E. Schulson for many fruitful discussions about ice friction experiments, and C. Marone and the Penn State Rock Mechanics group for development of XLook, which was used to analyse the data reported here. Reviews from two anonymous reviewers improved the manuscript.

## References

1. Sergienko OV, Hindmarsh RCA. 2013 Regular patterns in fricitonal resistance of ice-stream beds seen by surface data inversion. *Science* **342**, 1086–1089. (doi:10.1126/science.1243903)
2. Raymond CF, Harrison WD. 1987 Fit of ice motion models to observations from ariegated Glacier, Alaska. In *The physical basis of ice sheet modeling*, pp. 153–166. IAHS Publication no. 170. See http://hydrologie.org/redbooks/a170/iahs_170_0000.pdf.
3. Kamb B. 1991 Rheological nonlinearity and flow instability in the deforming bed mechanism of ice stream motion. *J. Geophys. Res.* **96**, 16 585–16 595. (doi:10.1029/91JB00946)
4. Bougamont M, Tulaczyk S, Joughin I. 2003 Numerical investigations of the slow-down of Whillans Ice Stream, West Antarctica: Is it shutting down like Ice Stream C? *Ann. Glaciol.* **37**, 239–246. (doi:10.3189/172756403781815555)
5. Zoet LK, Anandakrishnan S, Alley RB, Nyblade AA, Wiens DA. 2012 Motion of an Antarctic glacier by repeated tidally modulated earthquakes. *Nat. Geosci.* **5**, 623–626. (doi:10.1038/ngeo1555)
6. Luthra T, Anandakrishnan S, Winberry JP, Alley RB. 2016 Basal characteristics of the main sticky spot on the ice plain of Whillans Ice Stream. *Antarctica, EPSL* **440**, 12–19. (doi:10.1016/j.epsl.2016.01.035)
7. Cuffey KM, Paterson WSB. 2010 *The physics of glaciers*, 4th edn. Amsterdam, The Netherlands: Elsevier Inc.
8. Oksanen P, Keinonen J. 1982 The mechanism of friction of ice. *Wear* **78**, 315–324. (doi:10.1016/0043-1648(82)90242-3)
9. Beeman M, Durham WB, Kirby SH. 1988 Friction of ice. *J. Geophys. Res.* **93**, 7625–7633. (doi:10.1029/JB093iB07p07625)
10. Rist MA. 1997 High-stress ice fracture and friction. *J. Phys. Chem. B* **101**, 6263–6266. (doi:10.1021/jp963175x)
11. Kennedy FE, Schulson EM, Jones DE. 2000 The friction of ice on ice at low sliding velocities. *Philos. Mag. A* **80**, 1093–1110. (doi:10.1080/01418610008212103)
12. Schulson EM, Fortt AL. 2012 Friction of ice on ice. *J. Geophys. Res.* **117**, B12204. (doi:10.1029/2012JB009219)
13. Montagnat M, Schulson EM. 2003 On friction and surface cracking during sliding of ice on ice. *J. Glaciol.* **49**, 391–396. (doi:10.3189/172756503781830647)

14. Lishman B, Sammonds P, Feltham D. 2011 A rate and state friction law for saline ice. *J. Geophys. Res.* **116**, C05011. (doi:10.1029/2010JC006334)
15. Barnes P, Tabor D, Walker JCF. 1971 The friction and creep of polycrystalline ice. *Proc. R. Soc. Lond. A* **324**, 127–155. (doi:10.1098/rspa.1971.0132)
16. Zoet LK, Carpenter B, Scuderi M, Alley RB, Anandakrishnan S, Marone C, Jackson M. 2013 The effects of entrained debris on the basal sliding stability of a glacier. *J. Geophys. Res. Earth Surface* **118**, 656–666. (doi:10.1002/jgrf.20052)
17. Zoet LK, Iverson NR. 2015 Experimental determination of a double-valued drag relationship for glacier sliding. *J. Glaciol.* **61**, 1–7. (doi:10.3189/2015JoG14J174)
18. Rathbun AP, Marone C, Alley RB, Anandakrishnan S. 2008 Laboratory study of the frictional rheology of sheared till. *J. Geophys. Res.* **113**, F02020. (doi:10.1029/2007JF000815)
19. Dieterich JH. 1978 Time-dependent friction and the mechanics of stick-slip. *Pure Appl. Geophys.* **116**, 790–806. (doi:10.1007/BF00876539)
20. Dieterich JH. 1979 Modeling of rock friction, 1. Experimental results and constitutive equations. *J. Geophys. Res.* **84**, 2169–2175. (doi:10.1029/JB084iB05p02169)
21. Ruina A. 1983 Slip instability and state variable friction laws. *J. Geophys. Res.* **88**, 10 359–10 370. (doi:10.1029/JB088iB12p10359)
22. Marone C. 1998 Laboratory-derived friction laws and their application to seismic faulting. *Annu. Rev. Earth Planet. Sci.* **26**, 643–696. (doi:10.1146/annurev.earth.26.1.643)
23. Noda H, Lapusta N. 2013 Stable creeping fault segments can become destructive as a result of dynamic weakening. *Nature* **493**, 518–521. (doi:10.1038/nature11703)
24. Marone C, Vidale JE, Ellsworth WL. 1995 Fault healing inferred from time dependent variations in source properties of repeating earthquakes. *Geophys. Res. Lett.* **22**, 3095–3098. (doi:10.1029/95GL03076)
25. Marone CJ, Scholz CH, Bilham R. 1991 On the mechanics of earthquake afterslip. *J. Geophys. Res.* **96**, 8441–8452. (doi:10.1029/91JB00275)
26. Liu Y, Rice JR. 2005 Aseismic slip transients emerge spontaneously in three-dimensional rate and state modeling of subduction earthquake sequences. *J. Geophys. Res.* **110**, B08307. (doi:10.1029/2004JB003424)
27. Rabinowicz E. 1951 The nature of the static and kinetic coefficients of friction. *J. Appl. Phys.* **22**, 1373. (doi:10.1063/1.1699869)
28. Chester FM. 1994 Effects of temperature on friction: constitutive equations and experiments with quartz gouge. *J. Geophys. Res.* **99**, 7247–7261. (doi:10.1029/93JB03110)
29. Ikari MJ, Carpenter BM, Marone C. 2016 A microphysical interpretation of rate- and state-dependent friction for fault gouge. *Geochem. Geophys. Geosyst.* **17**, 1660–1677. (doi:10.1002/2016GC006286)
30. Cole DM. 1979 Preparation of polycrystalline ice specimens for laboratory experiments. *Cold Reg. Sci. Technol.* **1**, 153–159. (doi:10.1016/0165-232X(79)90007-7)
31. McCarthy C, Savage H, Koczynski T, Nielson M. 2016 An apparatus to measure frictional, anelastic, and viscous behavior in ice at temperate and planetary conditions. *Rev. Sci. Inst.* **87**, 055112. (doi:10.1063/1.4950782)
32. Reinan LA, Weeks JD. 1993 Determination of rock friction constitutive parameters using an iterative least-squares inversion method. *J. Geophys Res.* **98**,15 937–15 950. (doi:10.1029/93JB00780)
33. Scholz CH. 2002 *The mechanics of earthquakes and faulting*, 2nd edn. New York, NY: Cambridge University Press.
34. Tatinclaux JC. 1989 Effects of normal pressure on kinetic friction coefficient: myth or reality? In *Proc. of 22nd American Towing Tank Conf., St. John's, Newfoundland, Canada, 8–11 August 1989*, pp. 127–134. Ottawa, Canada: Ontario National Research Council of Canada.
35. Dieterich JH. 1972 Time-dependent friction in rocks. *J. Geophys. Res.* **77**, 3690–3697. (doi:10.1029/JB077i020p03690)
36. Beeler NM, Tullis TE, Weeks JD. 1994 The roles of time and displacement in evolution effect in rock friction. *Geophys. Res. Lett.* **21**, 1987–1990. (doi:10.1029/94GL01599)
37. Schindelin J *et al.* 2012 Fiji: an open-source platform for biological-image analysis. *Nat. Methods* **9**, 676–682. (doi:10.1038/nmeth.2019)
38. Schneider CA, Rasband WS, Eliceiri KW. 2012 NIH Image to ImageJ: 25 years of image analysis. *Nat. Methods* **9**, 671–675. (doi:10.1038/nmeth.2089)

39. Carpenter BM, Ikari MJ, Marone C. 2016 Laboratory observations of time-dependent strengthening and stress relaxation in natural and synthetic fault gouges. *J. Geophys. Res. Solid Earth* **121**, 1183–1201. (doi:10.1002/2015JB012136)
40. Bowden TP, Hughes FP. 1939 The mechanism of sliding on ice and snow. *Proc. R. Soc. Lond. A* **172**, 280–298. (doi:10.1098/rspa.1939.0104)
41. Maeno N, Arakawa M. 2004 Adhesion shear theory of ice friction at low sliding velocities, combined with ice sintering. *J. Appl. Phys*. **94**, 134–139. (doi:10.1063/1.1633654)
42. Marmo BA, Blackford JR, Jeffree CD. 2005 Ice friction, wear features and their dependence on sliding velocity and temperature. *J. Glaciol*. **51**, 391–398. (doi:10.3189/172756505781829304)
43. Rignot E, Velicogna I, van den Broeke MR, Monaghan A, Lenaerts J. 2011 Acceleration of the contribution of the Greenland and Antarctic ice sheets to sea level rise. *Geophys. Res. Lett*. **38**, L05503. (doi:10.1029/2011GL047109)
44. Rignot E, Box JE, Burgess E, Hanna E. 2008 Mass balance of the Greenland ice sheet from 1958 to 2007. *Geophys. Res. Lett.* **35**, L20502. (doi:10.1029/2008GL035417)
45. Blanpied ML, Lockner DA, Byerlee JD. 1995 Frictional slip of granite at hydrothermal conditions. *J. Geophys. Res*. **100**, 13 045–13 064. (doi:10.1029/95JB00862)
46. Mitchell EK, Fialko Y, Brown KM. 2013 Temperature dependence of frictional healing of Westerly granite: experimental observations and numerical simulations. *Geochem. Geophys. Geosyst*. **14**, 567–582. (doi:10.1029/2012GC004241)
47. Verberne BA, Niemeijer AR, De Bresser JHP, Spiers CJ. 2015 Mechanical behavior and microstructure of simulated calcite gouge sheared at 20–600°C: implications for natural faults in limestones. *J. Geophys. Res Solid Earth* **120**, 8169–8196. (doi:10.1002/2015JB012292)
48. Den Hartog SAM, Peach CJ, de Winter DAM, Spiers CJ. 2012 Frictional properties of megathrust fault gouges at low sliding velocities: new data on effects of normal stress and temperature. *J. Struct. Geol.* **38**, 156–171. (doi:10.1016/j.jsg.2011.12.001)
49. Sukhorukov S, Loset S. 2013 Friction of sea ice on sea ice. *Cold Reg. Sci. Technol* **94**, 1–12. (doi:10.1016/j.coldregions.2013.06.005)
50. Katayama I, Mutsumi I, Okazaki K, Hiauchi K. 2013 Slow earthquakes associated with fault healing on a serpentinized plate interface. *Nat. Sci. Rep*. **3**, 1784. (doi:10.1038/srep01784)
51. Nakatani M. 2001 Conceptual and physical clarification of rate and state friction: frictional sliding as a thermally activated rheology. *J. Geophys. Res*. **106**, 13347. (doi:10.1029/2000JB900453)
52. Schulson EM. 2015 Low-speed friction and brittle compressive failure of ice: fundamental processes in ice mechanics. *Int. Mat. Rev.* **60**, 8. (doi:10.1179/1743280415Y.0000000010)
53. Anandakrishnan S, Bentley CR. 1993 Micro-earthquakes beneath Ice Streams B and C, West Antarctica: observations and implications. *J. Glaciol*. **39**, 455–462.
54. Anandakrishnan S, Alley RB. 1997 Tidal forcing of basal seismicity of Ice Stream C, West Antarctica, observed far inland. *J. Geophys. Res.* **102**, 15 183–15 196. (doi:10.1029/97JB01073)
55. Danesi S, Bannister S, Morelli A. 2007 Repeating earthquakes from rupture of an asperity under an Antarctic outlet glacier. *Earth Planet. Sci. Lett*. **253**, 151–158. (doi:10.1016/j.epsl.2006.10.023)
56. Walter F, Deichmann N, Funk M. 2008 Basal icequakes during changing subglacial water pressures beneath Gornergletscher, Switzerland. *J. Glaciol*. **54**, 511–521. (doi:10.3189/002214308785837110)
57. Walter F, Dalban Canassy P, Husen S, Clinton JF. 2013 Deep icequakes: what happens at the base of Alpine glaciers? *J. Geophys. Res.* **118**, 1720–1728. (doi:10.1002/jgrf.20124)
58. Bindschadler RA, King MA, Alley RB, Anandakrishnan S, Padman L. 2003 Tidally controlled stick-slip discharge of a West Antarctic Ice Stream. *Science* **301**, 1087–1089. (doi:10.1126/science.1087231)
59. Wiens DA, Anandakrishnan S, Winberry JP, King MA. 2008 Simultaneous teleseismic and geodetic observations of the stick-slip motion of an Antarctic ice stream. *Nature* **453**, 770–774. (doi:10.1038/nature06990)
60. Winberry JP, Anandakrishnan S, Alley RB, Bindschadler RA, King MA. 2009 Basal mechanics of ice streams: insights from the stick-slip motion of Whillans Ice Stream, West Antarctica. *J. Geophys. Res.* **114**, F01016. (doi:10.1029/2008JF001035)
61. Winberry JP, Anandakrishan S, Alley RB, Wiens DA, Pratt MJ. 2014 Tidal pacing, skipped slips and the slowdown of Whillans Ice Stream, Antarctica. *J. Glaciol*. **60**, 795–807. (doi:10.3189/2014JoG14J038)

62. Pratt MJ, Winberry JP, Wiens DA, Anandakrishnan S, Alley RB. 2014 Seismic and geodetic evidence for grounding-line control of Whillans Ice Stream stick-slip events. *J. Geophys. Res.* **119**, 333–348. (doi:10.1002/2013JF002842)
63. Goldberg DN, Schoof C, Sergienko OV. 2014 Stick-slip motion of an Antarctic Ice Stream: the effects of viscoelasticity. *J. Geophys. Res*. **119**, 1564–1580. (doi:10.1002/2014JF003132)
64. Walker RT, Parizek BR, Alley RB, Anandakrishnan S, Riverman KL, Christianson K. 2013 Ice-shelf tidal flexure and subglacial pressure variations. *Earth Planet. Sci. Lett*. **361**, 422–428. (doi:10.1016/j.epsl.2012.11.008)